Biomedical Signal Processing and Control 8 (2013) 992–999

Contents lists available at ScienceDirect

Biomedical Signal Processing and Control

journal homepage: www.elsevier.com/locate/bspc

Atrial flutter and atrial tachycardia detection using Bayesian approach with high resolution time–frequency spectrum from ECG recordings

Jinseok Lee[a,*], David D. McManus[c], Peter Bourrell[c], Leif Sörnmo[d], Ki H. Chon[b]

[a] Department of Biomedical Engineering, Wonkwang University School of Medicine, Iksan, Jeonbuk, Republic of Korea
[b] Department of Biomedical Engineering, Worcester Polytechnic Institute, MA 01609, USA
[c] Cardiology Division, Departments of Medicine and Quantitative Health Sciences, University of Massachusetts Medical Center, Worcester, MA 01605 USA
[d] Signal Processing Group, Department of Applied Electronics, Lund University, Box 118, S-221 00 Lund, Sweden

ARTICLE INFO

Article history:
Received 14 August 2012
Received in revised form 22 March 2013
Accepted 1 April 2013
Available online 10 May 2013

Keywords:
Atrial flutter
Atrial tachycardia
Particle filter
Dynamic ECG model
High resolution time–frequency spectrum
Variable frequency complex demodulation
Electrocardiogram

ABSTRACT

Contemporary methods of atrial flutter (AFL), atrial tachycardia (AT), and atrial fibrillation (AF) monitoring, although superior to the standard 12-lead ECG and symptom-based monitoring, are unable to accurately discriminate between AF, AFL and AT. Thus, there is a need to develop accurate, automated, and comprehensive atrial arrhythmia detection algorithms using standard ECG recorders. To this end, we have developed a sensitive and real-time realizable algorithm for accurate AFL and AT detection using any standard electrocardiographic recording. Our novel method for automatic detection of atrial flutter and atrial tachycardia uses a Bayesian approach followed by a high resolution time–frequency spectrum. We find the TQ interval of the electrocardiogram (ECG) corresponding to atrial activity by using a particle filter (PF), and analyze the atrial activity with a high resolution time–frequency spectral method: variable frequency complex demodulation (VFCDM). The rationale for using a high-resolution time–frequency algorithm is that our approach tracks the time-varying fundamental frequency of atrial activity, where AT is within 2.0–4.0 Hz, AFL is within 4.0–5.3 Hz and NSR is found at frequencies less than 2.0 Hz. For classifications of AFL ($n = 22$), AT ($n = 10$) and normal sinus rhythms (NSR) ($n = 29$), we found that our approach resulted in accuracies of 0.89, 0.87 and 0.91, respectively; the overall accuracy was 0.88.

1. Introduction

The atrial tachyarrythmias atrial flutter (AFL), atrial tachycardia (AT), and atrial fibrillation (AF) represent the most common class of heart rhythm disorders presenting to medical attention [1–2]. Many algorithms have been developed to detect AF and can be categorized as being based on RR interval (RRI) variability [3–11]. Specifically, their aim was to quantify markedly increased beat-to-beat variability RRI time series in AF. Consequently, most algorithms showed sensitivity and specificity values higher than 90% for AF detection. On the other hand, automatic detection of AFL and AT is more challenging and has been less studied since the RRI characteristics of AFL and AT are regular, and the acquisition of the atrial signal (F-wave) is required.

AFL is an atrial dysrythmia that generates a discernable P-wave, making it difficult to distinguish from normal sinus rhythm. Moreover, although AFL often results from distinct electrophysiologic mechanisms, namely focal automaticity and macro-reentry, the RR intervals and P wave morphologies associated with these arrhythmias are often quite similar. An atrial rhythm of approximately 130–240 waves/min (i.e. 2.2–4 Hz) is referred to as AT while a regular macroreentrant atrial rhythm of approximately 240–320 waves (i.e. 4–5.3 Hz) is referred to as AFL [12]. Thus, the QRST cancelation or elimination (ventricular cancelation or elimination) in the ECG is critical for classification of AFL and AT by analyzing the atrial activity. In the TQ interval, electrical activity in the ECG is dominated by the atrial contribution while the ventricular component is a time series with missing data in the QT interval. The atrial signal is considered as a time series with missing data in the QT interval [13]. Some of the notable algorithms for QRST cancelation include spatiotemporal, the QRST cancelation technique, and average beat subtraction, but these require long ECG recordings (e.g. one minute of average beats or longer) [14–15]. Wave rectification, blind source separation, principal component analysis, and automatic mode switching are algorithms that have been developed to deal with the challenges of automated AT and AFL detection, but these methods are relatively crude, inconsistently effective, and with notable shortcomings [16–18]. Recently, Jacquemet et al. [19] proposed a new AFL detection algorithm, which reconstructs the spectrum of the atrial component of the

* Corresponding author. Tel.: +82 63 850 6973.
E-mail addresses: gonasago@wku.ac.kr, gonasago@gmail.com (J. Lee).

1746-8094/$ – see front matter © 2013 Elsevier Ltd. All rights reserved.
http://dx.doi.org/10.1016/j.bspc.2013.04.002

ECG corresponding to TQ intervals, but they assumed that the TQ intervals are given. Hence, at present, no reliable and complete AFL detection algorithm is available because existing QRST cancelation algorithms are insufficient as described above.

Recently, McSharry et al. introduced a powerful dynamic ECG model, which is capable of replicating many of the important features of the human ECG by generating different morphologies for the PQRST-complex [20]. Based on the dynamic model, Sayadi et al. [21] and Samenji et al. [22] used Kalman Filters (Extended Kalman Filter, Extended Kalman Smoother and Unscented Kalman Filter) as a Bayesian approach for ECG denoising and atrial activity analysis. Both demonstrated superior results compared with bandpass filtering, adaptive filtering, and wavelet transform over a wide range of ECG SNRs. We extended this concept to atrial signal (TQ interval) detection by using the Particle Filter (PF), which has been widely adopted in many estimation problems, as it is especially powerful for nonlinear and non-Gaussian problems [23–24]. It is widely known that the PF estimator performs better than any Kalman Filter estimator [25]. First, we modified the dynamic ECG model by generating only four waves for QRST (excluding P wave) complex, and predicted the prior density function by propagating parameters of peak amplitudes, peak widths, angular spreads and locations of each QRST wave. Since the ECG waveform itself and measurement noise are nonlinear and non-Gaussian, PF is more suitable than any Kalman Filter. Thus, our PF framework results in more accurate QRST wave detection than does a Kalman Filter algorithm. After finding the atrial signal, we use a high-resolution time-frequency method named variable frequency complex demodulation [27] in order to detect AFL and AT in the atrial signal.

2. Methods

2.1. Databases

We collected data from 22 AFL patients, 10 AT patients and 29 normal sinus rhythm (NSR) subjects. Electrocardiographic data were obtained from Holter recordings and retrospectively collected 12-lead electrocardiograms. Each ECG recording was approximately one to ten hours in duration. The University of Massachusetts Institutional Review Board approved the data collection and analysis of electrocardiographic data. Of participants with available clinical and demographic data, the mean age of participants with AFL was 69 ± 11 years of age and 57% were women. The mean age of participants with AT was 72 ± 13 years of age and 33% were women. The NSR data recordings were collected for 3 min using ScottCare RZ153 series recorders, and acquired at the sampling rate of 180 Hz with 10-bit resolution. The subjects were comprised of 15 men and 14 women, with a mean age of 24 ± 3.1 years. The NSR subjects were free from any known cardiovascular diseases.

2.2. Synthetic ECG model and TQ interval definition

Let us denote the onset of the Q wave by Q_{on}, and the end of the T wave by T_{end}. The TQ interval between T_{end} and Q_{on} corresponds to atrial activity. Then, the atrial activity signal $A_{TQ}(t)$ from ECG can be formulated as shown below:

$$A_{TQ}(t) = s(t) \cdot G_{TQ}(t), \tag{1}$$

where $s(t)$ is the measurement ECG, and $G_{TQ}(t)$ is a gating function defined as one in the intervals between T_{end} and Q_{on} and zero otherwise.

To find the end of the T wave (T_{end}) and the onset of the Q wave (Q_{on}), we used a synthetic ECG model [20] as follows:

$$\begin{cases} \dot{x} = \rho x - wy \\ \dot{y} = \rho y + wx \\ \dot{z} = \displaystyle\sum_{i \in \{P,Q,R,S,T\}} a_i \Delta\theta_i \exp\left(-\frac{\Delta\theta_i^2}{2b_i^2}\right) \end{cases} \tag{2}$$

where x, y and z are the state variables, $\rho = 1 - \sqrt{x^2 + y^2}$, $\Delta\theta_i = (\theta - \theta_i) \bmod (2\pi)$, $\theta = \text{atan2}(y,x)$ is the four quadrant arctangent of the elements of x and y with $0 \le \text{atan2}(y,x) \le 2\pi$, and w is the angular velocity of the trajectory as it moves around the limit cycle in x–y plane. The parameters a_i, b_i and θ_i represent peak amplitude, standard deviation (SD) and location of each PQRST wave, respectively. Then, in each one cycle of ECG, T_{end} and Q_{on} can be approximately calculated as

$$T_{end} = \theta_T + \alpha_T \cdot b_T, \tag{3}$$

and

$$Q_{on} = \theta_Q - \alpha_Q \cdot b_Q. \tag{4}$$

where α_T and α_Q are multiplication factors to determine T and Q wave half-width. That is, T_{end} can be calculated by the summation of T wave peak location ($\Delta\theta_T$) and the half-width ($\alpha_T \cdot b_T$). Similarly, Q_{on} can be calculated by the subtraction of Q wave peak location ($\Delta\theta_Q$) and the half-width ($\alpha_Q \cdot b_Q$). Since Eq. (2) assumes each wave is Gaussian form, the onset and end locations can be determined based on a confidence level. Under the confidence level of 0.99, we set up α_T and α_Q as 2.576.

2.3. TQ interval detection with particle filter

Given one cycle of ECG signal $s_{cycle}(t_1 : t_2)$, where t_1 and t_2 are each consecutive R peak time, we convert the time series $s_{cycle}(t_1 : t_2)$ to phase series $s_{cycle}(\theta, n)$, which is considered a measurement vector at the n-th cycle. The measurement vector $s_{cycle}(\theta, n)$ can be formulated by each PQRST peak amplitude, SD and location as follows:

$$s_{cycle}(\theta, n) = F(a_{i,n}, \theta_{i,n}, b_{i,n}, a_{u_i,n}, b_{u_i,n}, \theta_{u_i,n}), \quad i \in \{P, Q, R, S, T\} \tag{5}$$

where $F(\cdot)$ is a measurement function, where $a_{i,n}$, $\theta_{i,n}$ and $b_{i,n}$ form a sum of Gaussian functions with measurement noise $a_{u_i,n}$, $b_{u_i,n}$ and $\theta_{u_i,n}$ at the n-th cycle. Note that the measurement noise can be positive or negative. The measurement noise distorts the ECG morphology due to physical factors such as digitization errors, noise artifact and inaccurate R peak detection. Note that i represents each PQRST wave. Then, $s_{cycle}(\theta, n)$ can be expressed as

$$s_{cycle}(\theta, n) = \sum_{i \in \{P,Q,R,S,T\}} (a_{i,n} + a_{u_i,n}) \cdot (\Delta\theta_{i+u_i,n}) \cdot \exp\left(-\frac{(\Delta\theta_{i+u_i,n})^2}{2(b_{i,n} + b_{u_i,n})^2}\right), \tag{6}$$

where $\Delta\theta_{i+u_i,n} = (\theta - (\theta_{i,n} + \theta_{u_i,n})) \bmod (2\pi)$.

The QT interval includes both ventricular depolarization and repolarization. We define the ventricular activity by $\boldsymbol{M}(n)$

$$\boldsymbol{M}(n) = [\boldsymbol{Q}(n)\boldsymbol{R}(n)\boldsymbol{S}(n)\boldsymbol{T}(n)]^T, \tag{7}$$

where

$$\boldsymbol{Q}(n) = [a_{Q,n} b_{Q,n} \theta_{Q,n}],$$

$$\boldsymbol{R}(n) = [a_{R,n} b_{R,n} \theta_{R,n}],$$

$$\boldsymbol{S}(n) = [a_{S,n} b_{S,n} \theta_{S,n}],$$

and

$$\boldsymbol{T}(n) = [a_{T,n} b_{T,n} \theta_{T,n}].$$

We assume that the ventricular activity follows a Markov process, which can be modeled by activity transition relations as

$$\boldsymbol{M}(n) = \boldsymbol{T}(\boldsymbol{M}(n-1), \quad \boldsymbol{V}_{\text{int}}(n)) = \boldsymbol{M}(n-1) + \boldsymbol{V}_{\text{int}}(n), \tag{8}$$

where $T(\cdot)$ is an activity transition function that $\boldsymbol{M}(n)$ evolves over each cycle, and the evolution is associated with $\boldsymbol{V}_{\text{int}}(n)$. $\boldsymbol{V}_{\text{int}}(n)$ represents physiological parameters that changes the ECG morphology over each cycle (ex. respiratory sinus arrhythmia, metabolism and dysrhythmia) and can be expressed as

$$\boldsymbol{V}_{\text{int}}(n) = [\boldsymbol{v}_Q(n) \boldsymbol{v}_R(n) \boldsymbol{v}_S(n) \boldsymbol{v}_T(n)]^T, \tag{9}$$

where

$$\boldsymbol{v}_Q(n) = [a_{v_Q,n} b_{v_Q,n} \theta_{v_Q,n}],$$

$$\boldsymbol{v}_R(n) = [a_{v_R,n} b_{v_R,n} \theta_{v_R,n}],$$

$$\boldsymbol{v}_S(n) = [a_{v_S,n} b_{v_S,n} \theta_{v_S,n}],$$

and

$$\boldsymbol{v}_T(n) = [a_{v_T,n} b_{v_T,n} \theta_{v_T,n}].$$

Here, $a_{v_Q,n}$, $a_{v_R,n}$, $a_{v_S,n}$ and $a_{v_T,n}$ are the Q, R, S and T wave amplitude variations, $b_{v_Q,n}$, $b_{v_R,n}$, $b_{v_S,n}$, and $b_{v_T,n}$ are the Q, R, S and T wave width variations, and $\theta_{v_Q,n}$, $\theta_{v_R,n}$, $\Delta\theta_{v_S,n}$ and $\theta_{v_T,n}$ are the Q, R, S and T wave peak locations. Then $\boldsymbol{M}(n)$ can be expressed as

$$\begin{aligned}\boldsymbol{M}(n) &= [\boldsymbol{Q}(n-1)\boldsymbol{R}(n-1)\boldsymbol{S}(n-1)\boldsymbol{T}(n-1)]^T + [\boldsymbol{v}_Q(n)\boldsymbol{v}_R(n)\boldsymbol{v}_S(n)\boldsymbol{v}_T(n)]^T \\ &= \begin{bmatrix} a_{Q,n-1} + a_{v_Q,n} & b_{Q,n-1} + b_{v_Q,n} & \theta_{Q,n-1} + \theta_{v_Q,n} \\ a_{R,n-1} + a_{v_R,n} & b_{R,n-1} + b_{v_R,n} & \theta_{R,n-1} + \theta_{v_R,n} \\ a_{S,n-1} + a_{v_S,n} & b_{S,n-1} + b_{v_S,n} & \theta_{S,n-1} + \theta_{v_S,n} \\ a_{T,n-1} + a_{v_T,n} & b_{T,n-1} + b_{v_T,n} & \theta_{T,n-1} + \theta_{v_T,n} \end{bmatrix}\end{aligned} \tag{10}$$

Let $s_{cycle}(\theta, 1:n) = [s_{cycle}(\theta, 1) \ldots s_{cycle}(\theta, n-1) s_{cycle}(\theta, n)]$ denote the concatenation of all measurement vectors up to the n-th cycle. The aim is to recursively estimate the conditional posterior probability density $p(\boldsymbol{M}(n)|s_{cycle}(\theta, 1:n))$, from which the ventricular activity can be obtained from the mean values of the density function. We modified the dynamic ECG model by generating only four waves for QRST (excluding P wave) complex, and predicted prior density function by propagating parameters of peak amplitudes, peak widths, angular spreads and locations of each QRST wave. Details concerning the generic PF algorithm are described in [25–26].

Assuming that the posterior probability density at the $(n-1)$-th cycle is available, the posterior probability density at the n-th cycle can be found through the Chapman–Kolmogorov equation and Bayes' rule:

$$\begin{aligned} &p(\boldsymbol{M}(n)|s_{cycle}(\theta, 1:n-1)) \\ &= \int p(\boldsymbol{M}(n)|\boldsymbol{M}(n-1)) p(\boldsymbol{M}(n-1)|s_{cycle}(\theta, 1:n-1)) \cdot d\boldsymbol{M}(n-1), \end{aligned} \tag{11}$$

$$p(\boldsymbol{M}(n)|s_{cycle}(\theta, 1:n)) \propto p(s_{cycle}(\theta, n)|\boldsymbol{M}(n)) p(\boldsymbol{M}(n)|s_{cycle}(\theta, 1:n-1)), \tag{12}$$

where $p(\boldsymbol{M}(n)|s_{cycle}(\theta, 1:n-1))$ is the posterior probability density, $p(\boldsymbol{M}(n)|\boldsymbol{M}(n-1))$ is the state transition density, $p(\boldsymbol{M}(n)|s_{cycle}(\theta, 1:n))$ is the prediction probability density and $p(s_{cycle}(\theta, n)|\boldsymbol{M}(n))$ is the likelihood.

The first step to particle generation is to represent a prior probability density function $p(\boldsymbol{M}(n)|s_{cycle}(\theta, 1:n-1))$ by a set of particles To find the end of the T wave (T_{end}) and the onset of the Q wave (Q_{on}), we generate particles by using a synthetic ECG model in Eq. (2) without a P wave. In each one cycle of the ECG, the parameters a_i, b_i and θ_i are estimated and QRST waves are subsequently generated. Given the particles corresponding to the posterior probability density function of $p(\boldsymbol{M}(n-1)|s_{cycle}(\theta, 1:n-1))$ obtained at the $(n-1)$-th cycle, new particles $M^j(n)$ are generated at the n-th cycle as

$$\begin{aligned} &p(\boldsymbol{M}(n)|s_{cycle}(\theta, 1:n-1)) \sim \boldsymbol{M}^j(n) \\ &= \begin{bmatrix} a^j_{Q,n} & b^j_{Q,n} & \theta^j_{Q,n} \\ a^j_{R,n} & b^j_{R,n} & \theta^j_{R,n} \\ a^j_{S,n} & b^j_{S,n} & \theta^j_{S,n} \\ a^j_{T,n} & b^j_{T,n} & \theta^j_{T,n} \end{bmatrix} \\ &= \tilde{\boldsymbol{M}}^j(n-1) + \boldsymbol{V}^j_{\text{int}}(n), \quad j = \{1, 2, \ldots, J\} \end{aligned} \tag{13}$$

where $\boldsymbol{M}^j(n)$ and $\tilde{\boldsymbol{M}}^j(n)$ are the j-th generated particles and resampled particles, respectively, $j = \{1, 2, \ldots, J\}$ for the number of particles J. The generated particles $\boldsymbol{M}^j(n)$ can be expressed as

$$\begin{aligned} \boldsymbol{M}^j(n) &= [\tilde{\boldsymbol{Q}}^j(n-1)\tilde{\boldsymbol{R}}^j(n-1)\tilde{\boldsymbol{S}}^j(n-1)\tilde{\boldsymbol{T}}^j(n-1)]^T \\ &\quad + [\boldsymbol{v}^j_Q(n)\boldsymbol{v}^j_R(n)\boldsymbol{v}^j_S(n)\boldsymbol{v}^j_T(n)]^T \sim \sum_{i \in \{\boldsymbol{Q}, \boldsymbol{R}, \boldsymbol{S}, \boldsymbol{T}\}} (\tilde{a}^j_{i,n-1} + a^j_{v_i,n}) \\ &\quad \cdot (\widetilde{\Delta\theta}^j_{i+v_i,n}) \cdot \exp\left(-\frac{(\widetilde{\Delta\theta}^j_{i+v_i,n})^2}{2(\tilde{b}^j_{i,n-1} + b^j_{v_i,n})^2} \right) \end{aligned} \tag{14}$$

where $\widetilde{\Delta\theta}^j_{i+v_i,n} = (\theta - (\theta^j_{i,n} + \theta^j_{v_i,n}))\text{mod}(2\pi)$.

The resampled particles $\tilde{\boldsymbol{M}}^j(n)$ can be expressed as

$$\begin{aligned} \tilde{\boldsymbol{M}}^j(n) &= [\tilde{\boldsymbol{Q}}^j(n-1)\tilde{\boldsymbol{R}}^j(n-1)\tilde{\boldsymbol{S}}^j(n-1)\tilde{\boldsymbol{T}}^j(n-1)]^T \\ &= \begin{bmatrix} \tilde{a}^j_{Q,n} & \tilde{b}^j_{Q,n} & \tilde{\theta}^j_{Q,n} \\ \tilde{a}^j_{R,n} & \tilde{b}^j_{R,n} & \tilde{\theta}^j_{R,n} \\ \tilde{a}^j_{S,n} & \tilde{b}^j_{S,n} & \tilde{\theta}^j_{S,n} \\ \tilde{a}^j_{T,n} & \tilde{b}^j_{T,n} & \tilde{\theta}^j_{T,n} \end{bmatrix} \end{aligned}$$

We assume that $s_{cycle}(\theta, n)$ is a stationary process denoted as

$$s_{cycle}(\theta, n) = s_{cycle}(\theta, n-1). \tag{15}$$

After the new particles corresponding to the prior probability density function in (13) and (14) are generated, each particle weight should be evaluated based on the measurement vector $s_{cycle}(\theta, n)$. The weighted particles represent the posterior probability density function of $p(\boldsymbol{M}(n)|s_{cycle}(\theta, 1:n))$. For the particle weight $w^j(n)$ evaluation, we calculated correlation between $\boldsymbol{M}^j(n)$ and $s_{cycle}(\theta, n)$ for $j = 1,2,\ldots J$:

$$w^j(n) = Corr(\boldsymbol{M}^j(n), s_{cycle}(\theta, n)) \tag{16}$$

where $Corr(\cdot)$ is the function of correlation. To find the TQ interval, we normalized the particle weight as

$$\bar{w}^j(n) = \frac{w^j(n)}{\sum_J^{j=1} w^j(n)}, \tag{17}$$

Table 1
Initial QRST parameters for particle generation.

Index (i)	R	S	T	Q
$\tilde{\theta}^j_{i,0}$	0	$\pi/12$	$\pi/2$	$23\pi/12$
$\tilde{a}^j_{i,0}$	30	−7.5	0.75	−5.0
$\tilde{b}^j_{i,0}$	0.1	0.1	0.4	0.1

and calculated the mean values as in (18), which estimate the TQ interval based on (3) and (4).

$$\dot{a}_{T,n} = \sum_{j=1}^{J} a^j_{T,n} \cdot \bar{w}^j(n) \tag{18-1}$$

$$\dot{b}_{T,n} = \sum_{j=1}^{J} b^j_{T,n} \cdot \bar{w}^j(n) \tag{18-2}$$

$$\dot{\theta}_{T,n} = \sum_{j=1}^{J} \theta^j_{T,n} \cdot \bar{w}^j(n) \tag{18-3}$$

$$\dot{a}_{Q,n} = \sum_{j=1}^{J} a^j_{Q,n} \cdot \bar{w}^j(n) \tag{18-4}$$

$$\dot{b}_{Q,n} = \sum_{j=1}^{J} b^j_{Q,n} \cdot \bar{w}^j(n) \tag{18-5}$$

$$\dot{\theta}_{Q,n} = \sum_{j=1}^{J} \theta^j_{Q,n} \cdot \bar{w}^j(n) \tag{18-6}$$

Based on the weighted particles, we resample them to generate new particles at the next cycle $n+1$ [25]. The overall algorithm is summarized below

1. Initial step ($n=1$)
   i) Predict the new set of particles $\boldsymbol{M}^j(1)$, where $j=1,2,\ldots J$ for the number of particles J.
   $$\boldsymbol{M}^j(1) = [\tilde{\boldsymbol{Q}}^j(0)\tilde{\boldsymbol{R}}^j(0)\tilde{\boldsymbol{S}}^j(0)\tilde{\boldsymbol{T}}^j(0)]^T + [\boldsymbol{v}^j_Q(1)\boldsymbol{v}^j_R(1)\boldsymbol{v}^j_S(1)\boldsymbol{v}^j_T(1)]^T,$$
   where $[\tilde{\boldsymbol{Q}}^j(0)\tilde{\boldsymbol{R}}^j(0)\tilde{\boldsymbol{S}}^j(0)\tilde{\boldsymbol{T}}^j(0)]^T$ is given in Table 1 [20].
   ii) Detect two adjacent R peaks and obtain measurement vector $s_{cycle}(\theta, 1)$.
   iii) Evaluate each particle weight $w^j(1) = Corr(\boldsymbol{M}^j(1), s_{cycle}(\theta, 1))$
   iv) Normalize the particle weight $\bar{w}^j(1) = (w^j(1))/(\sum_J^{j=1} w^j(1))$
   v) Calculate mean values and estimate TQ interval
   $T_{end} = \dot{\theta}_{T,1} + 2.576 \cdot \dot{b}_{T,1}$
   $Q_{on} = \dot{\theta}_{Q,1} - 2.576 \cdot \dot{b}_{Q,1}$
   vi) Resample particles $\tilde{\boldsymbol{M}}^j(1)$
2. From $n=2$
   i) Predict the new set of particles $\boldsymbol{M}^j(n)$, where $j=1,2,\ldots J$ for the number of particles J.
   $$\boldsymbol{M}^j(n) = [\tilde{\boldsymbol{Q}}^j(n-1)\tilde{\boldsymbol{R}}^j(n-1)\tilde{\boldsymbol{S}}^j(n-1)\tilde{\boldsymbol{T}}^j(n-1)]^T + [\boldsymbol{v}^j_Q(n)\boldsymbol{v}^j_R(n)\boldsymbol{v}^j_S(n)\boldsymbol{v}^j_T(n)]^T$$
   ii) Detect two adjacent R peaks and obtain measurement vector $s_{cycle}(\theta, n)$.
   iii) Evaluate each particle weight $w^j(n) = Corr(\boldsymbol{M}^j(n), s_{cycle}(\theta, n))$
   iv) Normalize the particle weight $\bar{w}^j(n) = (w^j(n))/(\sum_J^{j=1} w^j(n))$
   v) Calculate mean values and estimate TQ interval
   $T_{end} = \dot{\theta}_{T,n} + 2.576 \cdot \dot{b}_{T,n}$
   $Q_{on} = \dot{\theta}_{Q,n} - 2.576 \cdot \dot{b}_{Q,n}$
   vi) Resample particles $\tilde{\boldsymbol{M}}^j(n)$

Fig. 1 shows the instance of TQ interval estimation with one cycle of AFL samples. Fig. 1(a) shows one cycle of AFL samples (thick and red) and the generated particles (thin and blue). Fig. 1(b) shows the estimated QRST wave (thin and blue), where $\dot{a}_{T,n}$, $\dot{b}_{T,n}$, $\dot{\theta}_{T,n}$, $\dot{a}_{Q,n}$, $\dot{b}_{Q,n}$, $\dot{\theta}_{Q,n}$ are estimated. Based on the TQ interval definition of (3) and (4), we can obtain the atrial activity signal (P wave).

2.4. Atrial flutter detection using high resolution time-frequency spectrum

After obtaining the atrial activity signal, we analyzed the dominant frequency of the atrial activity by using variable frequency complex demodulation (VFCDM) method [27]. The VFCDM method showed higher resolution than any other time-frequency spectrum methods such as smoothed pseudo Wigner-Ville (SPWV) short time Fourier transform (STFT), and wavelet transform (WT) [27–29]. Consider a sinusoidal signal $x(t)$ to be a narrow band oscillation with a center frequency f_0, instantaneous amplitude $A(t)$, phase $\varphi(t)$, and the direct current component $dc(t)$:

$$x(t) = dc(t) + A(t)\cos(2\pi f_0 t + \varphi(t)) \tag{20}$$

For a given center frequency, we can extract the instantaneous amplitude information $A(t)$ and phase information $\varphi(t)$ by multiplying Eq. (1) by $e^{-j2\pi f_0 t}$ which results in the following:

$$z(t) = x(t)e^{-j2\pi f_0 t} = dc(t)e^{-j2\pi f_0 t} + \frac{A(t)}{2}e^{j\varphi(t)} + \frac{A(t)}{2}e^{-j(4\pi f_0 t + \varphi(t))} \tag{21}$$

A leftward shift by $e^{-j2\pi f_0 t}$ results in moving the center frequency, f_0, to zero frequency in the spectrum of $z(t)$. If $z(t)$ in (21) is subjected to an ideal low-pass filter (LPF) with a cutoff frequency $f_c < f_0$, then the filtered signal $z_{lp}(t)$ will contain only the component of interest and we obtain the following:

$$z_{lp}(t) = \frac{A(t)}{2}e^{j\varphi(t)} \tag{22}$$

$$A(t) = 2|z_{lp}(t)| \tag{23}$$

$$\varphi(t) = dc(t) + A(t)\cos\left(\int_0^t 2\pi f(\tau)d\tau + \phi(t)\right). \tag{24}$$

Similar to the operations in Eqs. (20) and (21), multiplying Eq. (6) by $e^{-j\int_0^t 2\pi f(\tau)d\tau}$ yields both instantaneous amplitude, $A(t)$, and instantaneous phase, $\varphi(t)$:

$$z(t) = x(t)e^{-j\int_0^t 2\pi f(\tau)d\tau} = dc(t)e^{-j\int_0^t 2\pi f(\tau)d\tau} + \frac{A(t)}{2}e^{j\varphi(t)} + \frac{A(t)}{2}e^{-j(\int_0^t 4\pi f(\tau)d\tau + \phi(t))} \tag{25}$$

From Eq. (25), if $z(t)$ is filtered with an ideal LPF with a cutoff frequency $f_c < f_0$, then the filtered signal $z_{lp}(t)$ will be obtained with the same instantaneous amplitude $A(t)$ and phase $\varphi(t)$ as provided in Eqs. (23) and (24). Details concerning the VFCDM algorithm are described in [26].

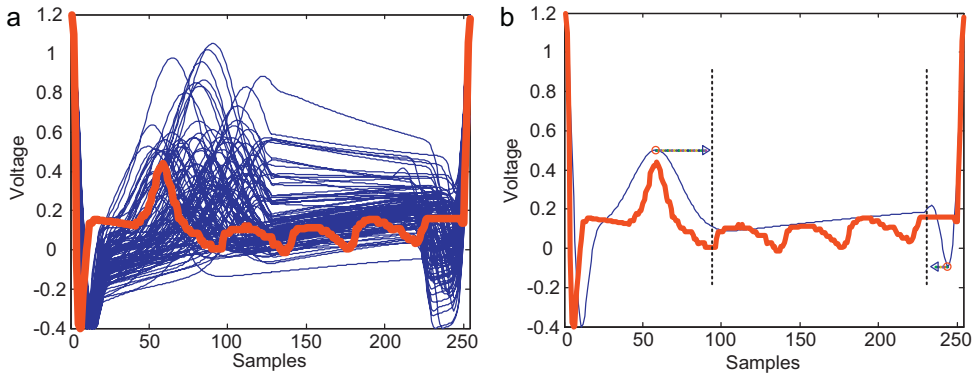

Fig. 1. Example (AFL): (a) generated QRST complex-particles (thick and red: AFL measurement, thin and blue: particles); (b) estimated wave for P wave extraction (thick and red: AFL measurement, thin and blue: final estimation). (For interpretation of the references to color in this figure legend, the reader is referred to the web version of this article.)

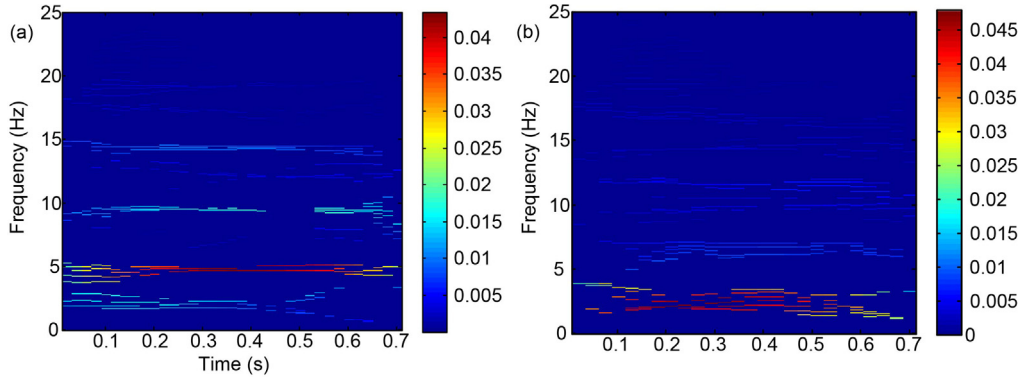

Fig. 2. Time–frequency analysis of (a) AFL atrial activity wave and (b) AT atrial activity wave.

Fig. 2 shows the resultant time-frequency spectrum of AFL and AT atrial activity. In Fig. 2(a), we used the AFL atrial activity wave obtained from Fig. 1(b), and the dominant frequencies were found around 4.8 Hz. Fig. 2(b) shows the time–frequency spectrum of AT atrial activity wave, and the dominant frequencies were found around 3 Hz.

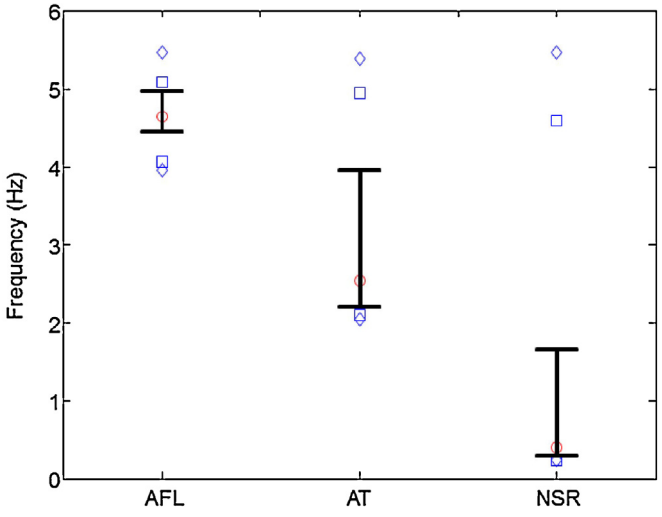

Fig. 3. Distribution of atrial activity wave dominant frequencies (sample to sample) on AFL, AT, and NSR databases. The diamonds above and below represent the 5th and the 95th percentiles of each different dataset, and the squares above and below represent the 90th and the 10th percentiles. Whiskers above and below represent the 75th and the 25th percentiles, respectively. The circle indicates the median value.

3. Results

3.1. Results from clinical database

Fig. 3 shows the sample-to-sample distribution of atrial activity wave dominant frequencies on AFL ($n = 22$), AT ($n = 10$) and NSR ($n = 29$) databases. For the simulation, we used 100 particles ($J = 100$). The diamonds above and below represent the 5th and the 95th percentiles of each different dataset, and the squares above and below represent the 90th and the 10th percentiles. Whiskers above and below represent the 75th and the 25th percentiles, respectively. The circles indicate the median value. For AFL, the median frequency was 4.64 Hz and the interquartile range was 0.54 Hz; the 25th percentile and the 75th percentile were 4.44 Hz and 4.98 Hz, respectively. For AT, the median frequency was 2.54 Hz and the interquartile range was 1.56 Hz; the 25th percentile and the 75th percentile were 2.30 Hz and 3.86 Hz, respectively. For NSR, the median frequency was 0.39 Hz and the interquartile range was 1.37 Hz; the 25th percentile and the 75th percentile were 0.29 Hz and 1.66 Hz, respectively.

To discriminate among AFL, AT, and NSR, we followed the procedure below:

- If $TH(AT,AFL) \leq$ frequency ≤ 5.4 Hz, then declare as AFL
- If $TH(NSR,AT) \leq$ frequency $< TH(AT,AFL)$, then declare as AT
- If frequency $< TH(NSR,AT)$, then declare as NSR
- Increment $TH(AT,AFL)$ from 3.0 to 5.0 Hz with an interval of 0.1 Hz
- Increment $TH(NSR,AT)$ from 1.0 to 3.0 Hz with an interval of 0.1 Hz
- Find ROC curves and the best pair of $TH(AT,AFL)$ and $TH(NSR,AT)$ providing the best accuracy

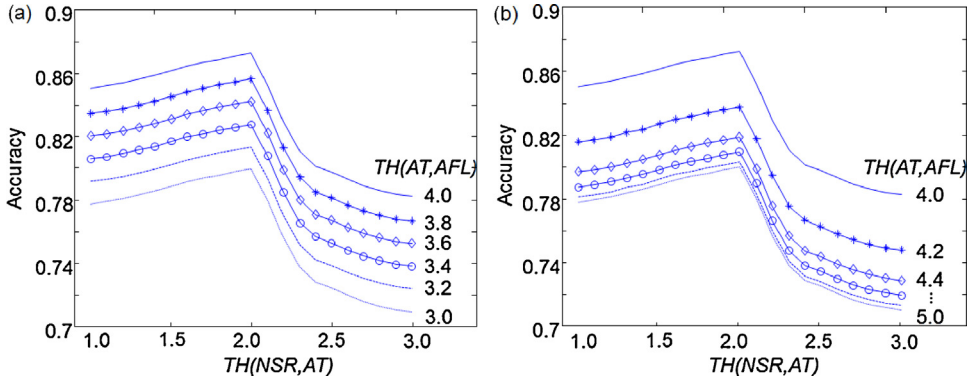

Fig. 4. Accuracy of AFL, AT, and NSR detection according to *TH*(*AT*,*AFL*) and *TH*(*AT*,*AFL*). It shows that *TH*(*AT*,*AFL*) = 4.0 and *TH*(*NSR*,*AT*) = 2.0 provided the best accuracy.

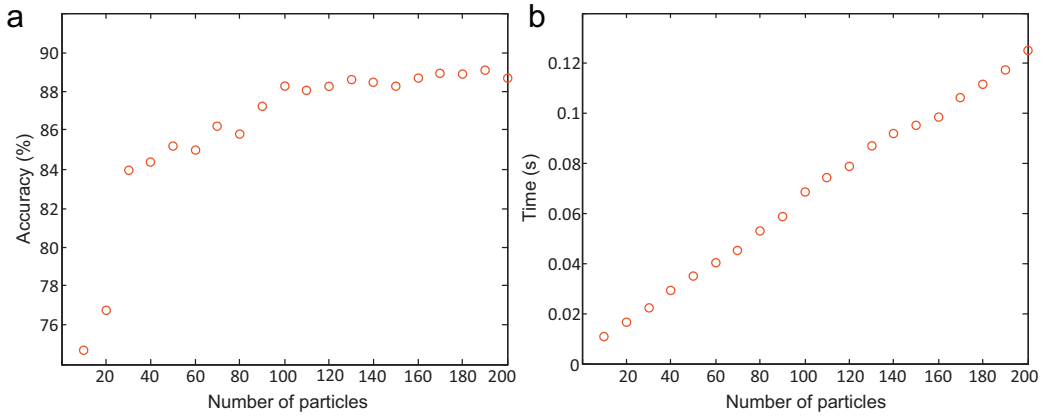

Fig. 5. Accuracy and computation time according to model orders.

Fig. 4 shows the accuracy of AFL, AT and NSR detection according to *TH*(*AT*,*AFL*) and *TH*(*NSR*,*AT*). It shows that *TH*(*AT*,*AFL*) = 4.0 and *TH*(*NSR*,*AT*) = 2.0 provided the best accuracy. For the AFL database, we found sensitivity of 0.89, specificity of 0.87 and accuracy of 0.89. For the AT database, we found sensitivity of 0.81, specificity of 0.92 and accuracy of 0.87. For the NSR database, we found sensitivity of 0.82, specificity of 0.99 and accuracy of 0.91.

Fig. 5 summarizes the detection accuracy and computation time as the number of particles varied from 10 to 200 with an interval of 10. Fig. 5(a) shows that the accuracy becomes constant when the number of particles approaches 90 or 100. On the other hand, Fig. 5(b) shows that the computation time linearly increases as the number of particles increases.

3.2. Analysis with synthesized ECG signals

To further analyze our algorithm, we used the synthetic ECG model in (2) to generate 50 realizations of AT and AFL signals. The sampling frequency was set to 200 Hz, mean heart rate to 150 bpm, standard deviation of heart rate to 1 bpm, and LF/HF ratio to 0.5. In addition, a_p, b_p and θ_p were set to [1.2 1.2], [0.25 0.25] and [$3\pi/2$ $11\pi/6$], respectively for AT, and a_p, b_p and θ_p were set to [1.2 1.2 1.2], [0.25 0.25 0.25] and [$3\pi/2$ $5\pi/3$ $11\pi/6$], respectively for AFL [12,20,30]. Each ECG signal realization was 1 min in duration and 100 particles were used for PF. Fig. 6 shows the resultant sample-to-sample distribution of atrial dominant frequencies of the synthesized AT and AFL signals. As shown in Fig. 6, for AT, the median frequency was 3.6 Hz, the 25th percentile was 3.1 Hz and the 75th percentile was 3.9 Hz. For AFL, the median frequency was 4.8 Hz, the 25th percentile was 4.4, and the 75th percentile was 5.0 Hz. Using the threshold values obtained from the clinical database, the classification accuracies of AT and AFL were 92.3% and 93.1%, respectively.

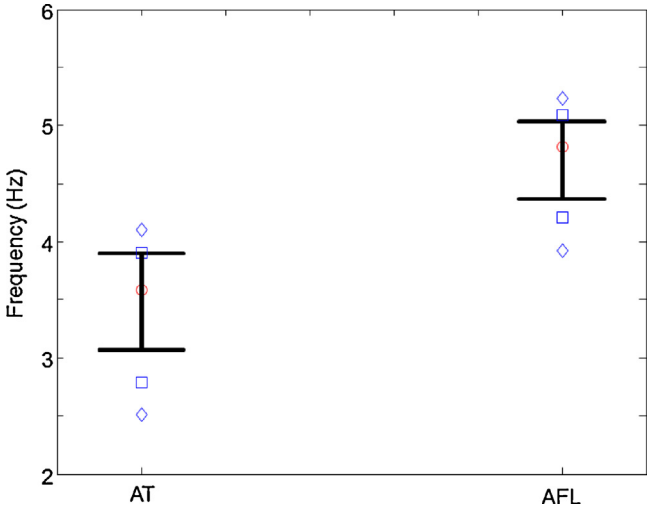

Fig. 6. Distribution of atrial activity wave dominant frequencies (sample to sample) of simulated AFL and AT signals. The diamonds above and below represent the 5th and the 95th percentiles of each different dataset, and the squares above and below represent the 90th and the 10th percentiles. Whiskers above and below represent the 75th and the 25th percentiles, respectively. The circles indicate the median values.

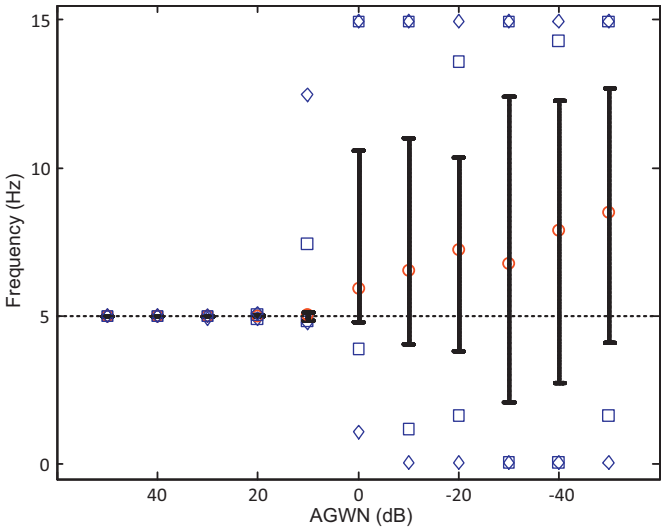

Fig. 7. Estimated frequencies of 5 Hz p-wave as a function of additive Gaussian white noise.

3.3. *Analysis of noise effect on P wave frequencies*

Fig. 7 shows the estimated dominant frequency effect from additive Gaussian white noise (GWN). For the analysis, we generated a clean synthetic ECG signal with 5 Hz atrial activity wave, and corrupted the signal by adding GWN. The simulation was performed 100 times for each SNR from −50 to 50 dB with an interval of 10 dB, and the estimated dominant frequency distribution was plotted in Fig. 7. The diamonds above and below represent the 5th and the 95th percentiles of each different dataset, and the squares above and below represent the 90th and the 10th percentiles. Whiskers above and below represent the 75th and the 25th percentiles, respectively. The circles indicate the median values. When the signal-to-noise ratio (SNR) was 20 dB or higher, all estimated dominant frequencies were 5 Hz. With 10 dB, 90% of dominant frequencies were 5 Hz. However, when SNR decreased to zero or below, the estimated dominant frequencies tended to be random.

4. Discussion and conclusion

In this paper, we presented a novel AFL and AT detection method by using particle filtration followed by the VFCDM method. The overall accuracy value was 0.88; 0.89 for AFL, 0.87 for AT and 0.91 for NSR. The most attractive feature of our approach is that it can be used to accurately find TQ intervals and detect AFL and AT in each R–R interval. In addition, our method is applicable for a Holter system as it is real-time realizable. Based on the average of multiple trials, the computation time was approximately 110 ms for 100 particles on Matlab 2011b on a 2.80 GHz Intel Core2 processor; 80 ms for PF and 30 ms for VFCDM. Our method works for ECG signals measured from at least 2 leads. However, it is known if our method works with single lead data.

Acknowledgment

This work was funded in part by the Office of Naval Research work unit N00014-08-1-0244.

References

[1] C. Blomstrom-Lundqvist, M.M. Scheinman, E.M. Aliot, J.S. Alpert, H. Calkins, A.J. Camm, W.B. Campbell, D.E. Haines, K.H. Kuck, B.B. Lerman, D.D. Miller, C.W. Shaeffer, W.G. Stevenson, G.F. Tomaselli, E.M. Antman, S.C. Smith, D.P. Faxon Jr., V. Fuster, R.J. Gibbons, G. Gregoratos, L.F. Hiratzka, S.A. Hunt, A.K. Jacobs, R.O. Russell, S.G. Priori Jr., J.J. Blanc, A. Budaj, E.F. Burgos, M. Cowie, J.W. Deckers, M.A. Garcia, W.W. Klein, J. Lekakis, B. Lindahl, G. Mazzotta, J.C. Morais, A. Oto, O. Smiseth, H.J. Trappe, ACC/AHA/ESC guidelines for the management of patients with supraventricular arrhythmias-executive summary: a report of the American College of Cardiology/American Heart Association Task Force on Practice Guidelines and the European Society of Cardiology Committee for Practice Guidelines (Writing Committee to Develop Guidelines for the Management of Patients with Supraventricular Arrhythmias) developed in collaboration with NASPE-Heart Rhythm Society, Journal of the American College of Cardiology 42 (8) (2003) 1493–1531, October 15.

[2] D.E. Krummen, M. Patel, H. Nguyen, G. Ho, D.S. Kazi, P. Clopton, M.C. Holland, S.L. Greenberg, G.K. Feld, M.N. Faddis, S.M. Narayan, Accurate ECG diagnosis of atrial tachyarrhythmias using quantitative analysis: a prospective diagnostic and cost-effectiveness study, Journal of Cardiovascular Electrophysiology 21 (November (11)) (2010) 1251–1259.

[3] M. Fukunami, T. Yamada, M. Ohmori, K. Kumagai, K. Umemoto, A. Sakai, N. Kondoh, T. Minamino, N. Hoki, Detection of patients at risk for paroxysmal atrial fibrillation during sinus rhythm by P wave-triggered signal-averaged electrocardiogram, Circulation 83 (January (1)) (1991) 162–169.

[4] G. Opolski, P. Scislo, J. Stanislawska, A. Gorecki, R. Steckiewicz, A. Torbicki, Detection of patients at risk for recurrence of atrial fibrillation after successful electrical cardioversion by signal-averaged P-wave ECG, International Journal of Cardiology 60 (2) (1997) 181–185, July 25.

[5] M. Budeus, M. Hennersdorf, C. Perings, B.E. Strauer, Detection of atrial late potentials with P wave signal averaged electrocardiogram among patients with paroxysmal atrial fibrillation, Zeitschrift fur Kardiologie 92 (May (5)) (2003) 362–369.

[6] D. Michalkiewicz, M. Dziuk, G. Kaminski, R. Olszewski, M. Cholewa, A. Cwetsch, L. Markuszewski, Detection of patients at risk for paroxysmal atrial fibrillation (PAF) by signal averaged P wave, standard ECG and echocardiography, Polski Merkuriusz Lekarski 20 (January (115)) (2006) 69–72.

[7] S. Dash, K.H. Chon, S. Lu, E.A. Raeder, Automatic real time detection of atrial fibrillation, Annals of Biomedical Engineering 37 (September (9)) (2009) 1701–1709.

[8] N. Kikillus, G. Hammer, N. Lentz, F. Stockwald, A. Bolz, Three different algorithms for identifying patients suffering from atrial fibrillation during atrial fibrillation free phases of the ECG, Computers in Cardiology 34 (2007) 801–804.

[9] B. Logan, J. Healey, Robust detection of atrial fibrillation for a long term telemmonitoring system, Computers in Cardiology 32 (2005) 619–622.

[10] K. Tateno, L. Glass, Automatic detection of atrial fibrillation using the coefficient of variation and density histograms of RR and deltaRR intervals, Medical and Biological Engineering and Computing 39 (November (6)) (2001) 664–671.

[11] C. Huang, S. Ye, H. Chen, D. Li, F. He, Y. Tu, A novel method for detection of the transition between atrial fibrillation and sinus rhythm, IEEE Transactions on Biomedical Engineering 58 (April (4)) (2011) 1113–1119.

[12] M. Stridh, A. Bollmann, S.B. Olsson, L. Sornmo, Detection and feature extraction of atrial tachyarrhythmias. A three stage method of time–frequency analysis, IEEE Engineering in Medicine and Biology Magazine 25 (November/December (6)) (2006) 31–39.

[13] R. Sassi, V.D. Corino, L.T. Mainardi, Analysis of surface atrial signals: time series with missing data? Annals of Biomedical Engineering 37 (October (10)) (2009) 2082–2092.

[14] J. Slocum, E. Byrom, L. McCarthy, A. Sahakian, S. Swiryn, Computer detection of atrioventricular dissociation from surface electrocardiograms during wide QRS complex tachycardias, Circulation 72 (November (5)) (1985) 1028–1036.

[15] M. Stridh, L. Sornmo, Spatiotemporal QRST cancellation techniques for analysis of atrial fibrillation, IEEE Transactions on Biomedical Engineering 48 (January (1)) (2001) 105–111.

[16] I. Christov, G. Bortolan, I. Daskalov, Automatic detection of atrial fibrillation and flutter by wave rectification method, Journal of Medical Engineering and Technology 25 (September/October (5)) (2001) 217–221.

[17] W.G. de Voogt, N.M. van Hemel, A.A. van de Bos, J. Koistinen, J.H. Fast, Verification of pacemaker automatic mode switching for the detection of atrial fibrillation and atrial tachycardia with Holter recording, Europace 8 (November (11)) (2006) 950–961.

[18] R.S. Passman, K.M. Weinberg, M. Freher, P. Denes, A. Schaechter, J.J. Goldberger, A.H. Kadish, Accuracy of mode switch algorithms for detection of atrial tachyarrhythmias, Journal of Cardiovascular Electrophysiology 15 (July (7)) (2004) 773–777.

[19] V. Jacquemet, B. Dube, R. Nadeau, A.R. LeBlanc, M. Sturmer, G. Becker, T. Kus, A. Vinet, Extraction and analysis of T waves in electrocardiograms during atrial flutter, IEEE Transactions on Biomedical Engineering 58 (April (4)) (2011) 1104–1112.

[20] P.E. McSharry, G.D. Clifford, L. Tarassenko, L.A. Smith, A dynamical model for generating synthetic electrocardiogram signals, IEEE Transactions on Biomedical Engineering 50 (March (3)) (2003) 289–294.

[21] O. Sayadi, M.B. Shamsollahi, G.D. Clifford, Synthetic ECG generation and Bayesian filtering using a Gaussian wave-based dynamical model, Physiological Measurement 31 (October (10)) (2010) 1309–1329.

[22] R. Sameni, M.B. Shamsollahi, C. Jutten, G.D. Clifford, A nonlinear Bayesian filtering framework for ECG denoising, IEEE Transactions on Biomedical Engineering 54 (December (12)) (2007) 2172–2185.

[23] J. Lee, K.H. Chon, Time-varying autoregressive model-based multiple modes particle filtering algorithm for respiratory rate extraction from pulse oximeter, IEEE Transactions on Biomedical Engineering 58 (March (3)) (2011) 790–794.

[24] J. Lee, K.H. Chon, An autoregressive model-based particle filtering algorithms for extraction of respiratory rates as high as 90 breaths per minute from pulse oximeter, IEEE Transactions on Biomedical Engineering 57 (September (9)) (2010) 2158–2167.
[25] M.S. Arulampalam, S. Maskell, N. Gordon, T. Clapp, A tutorial on particle filters for online nonlinear/non-Gaussian Bayesian tracking, IEEE Transactions on Signal Processing 50 (2) (2002) 174–188.
[26] G. Oppenheim, A. Philippe, J.D. Rigal, The particle filters and their applications, Chemometrics and Intelligent Laboratory Systems March (91) (2008) 87–93.
[27] H. Wang, K. Siu, K. Ju, K.H. Chon, A high resolution approach to estimating time–frequency spectra and their amplitudes, Annals of Biomedical Engineering 34 (February (2)) (2006) 326–338.
[28] K.H. Chon, S. Dash, K. Ju, Estimation of respiratory rate from photoplethysmogram data using time–frequency spectral estimation, IEEE Transactions on Biomedical Engineering 56 (August (8)) (2009) 2054–2063.
[29] N. Selvaraj, K. Shelley, D. Silverman, N. Stachenfeld, N. Galante, Y. Mendelson, J. Florian, K. Chon, A novel approach using time–frequency analysis of pulse-oximeter data to detect progressive hypovolemia in spontaneously breathing healthy subjects, IEEE Transactions on Biomedical Engineering 58 (August (8)) (2011) 2272–2279.
[30] K.W. Lee, Y. Yang, M.M. Scheinman, Atrial flutter: a review of its history, mechanisms, clinical features, and current therapy, Current Problems in Cardiology 30 (3) (2005) 121–167.